Tropomyosin Positions in Regulated Thin Filaments Revealed by Cryoelectron Microscopy

C. Xu*, R. Craig,# L. Tobacman,§ R. Horowitz,# and W. Lehman*

*Department of Physiology, Boston University School of Medicine, Boston, Massachusetts 02118 USA; #Department of Cell Biology, University of Massachusetts Medical School, Worcester, Massachusetts 01655 USA; and §Departments of Internal Medicine and Biochemistry, University of Iowa College of Medicine, Iowa City, Iowa 52242 USA

ABSTRACT Past attempts to detect tropomyosin in electron micrograph images of *frozen-hydrated* troponin-regulated thin filaments under relaxing conditions have not been successful. This raised the possibility that tropomyosin may be disordered on filaments in the off-state, a possibility at odds with the steric blocking model of muscle regulation. By using cryoelectron microscopy and helical image reconstruction we have now resolved the location of tropomyosin in both *relaxing* and *activating* conditions. In the off-state, tropomyosin adopts a position on the outer domain of actin with a binding site virtually identical to that determined previously by negative staining, although at a radius of 3.8 nm, slightly higher than found in stained filaments. Molecular fitting to the atomic model of F-actin shows that tropomyosin is localized over sites on actin subdomain 1 required for myosin binding. Restricting access to these sites would inhibit the myosin-cross-bridge cycle, and hence contraction. Under high Ca^{2+} activating conditions, tropomyosin moved azimuthally, away from its blocking position to the same site on the inner domain of actin previously determined by negative staining, also at 3.8 nm radius. These results provide strong support for operation of the steric mechanism of muscle regulation under near-native solution conditions and also validate the use of negative staining in investigations of muscle thin filament structure.

INTRODUCTION

Muscle contractility is widely thought to be controlled by movement of tropomyosin strands on actin-containing thin filaments. The assumption is that muscle relaxes because Ca^{2+}-free troponin constrains tropomyosin over strong myosin-binding sites on actin, blocking cross-bridge interaction and hence contraction (Holmes, 1995). After Ca^{2+} binds to troponin, tropomyosin movement away from the binding sites is followed by cross-bridge-actin interaction and contraction (Kress et al., 1986). This steric model of regulation was originally based on changes observed in x-ray diffraction patterns of intact skeletal muscle fibers (Haselgrove, 1972; Huxley, 1972; Parry and Squire, 1973). Further analysis, stimulated by the elucidation of atomic structures of F-actin (Holmes and Kabsch, 1991) and the actin-myosin interface (Rayment et al., 1993a, b; Holmes, 1997), has led to more detailed models while retaining the basic tenets originally proposed (AL-Khayat et al., 1995; Holmes, 1995; Lorenz et al., 1995; Poole et al., 1995). Direct support was obtained from electron microscopy and three-dimensional (3-D) image reconstruction of negatively stained isolated filaments in which tropomyosin was visualized directly in low and high Ca^{2+} states (Lehman et al., 1994, 1995; Vibert et al., 1997). Results of x-ray diffraction modeling and image reconstruction were mutually supportive, and tropomyosin positions were identical by both techniques (Lehman et al., 1994, 1995; Poole et al., 1995; Vibert et al., 1997). In the low Ca^{2+} (off)-state, tropomyosin was located on the surface of the outer domain of actin, obstructing access to several clusters of amino acids on subdomain 1 thought to be involved in strong stereospecific myosin-binding and required for the power stroke during the cross-bridge cycle (Lehman et al., 1994, 1995; Holmes, 1995; Lorenz et al., 1995; Poole et al., 1995; Vibert et al., 1997). Full switching-on of thin filaments and concomitant unblocking of myosin-binding sites was found to involve a two-step movement of tropomyosin to the inner domain of actin, dependent on Ca^{2+} and the binding of small numbers of myosin heads acting in sequence (Poole et al., 1995; Vibert et al., 1997). The three structural states of the thin filament identified (off-, Ca^{2+}-induced, myosin-induced) may correspond to three biochemically distinguished states (Bremel et al., 1972; Lehrer and Morris, 1982; McKillop and Geeves, 1993; Lehrer, 1994; Landis et al., 1997; Lehrer and Geeves, 1998).

Three-dimensional reconstruction of electron micrographs currently is the only direct way of visualizing tropomyosin strands on thin filaments, because micrograph images contain both intensity and requisite phase information. However, although reconstructions of negatively stained filaments reveal tropomyosin positions consistent with x-ray diffraction modeling, uncertainty remains concerning the effects of staining and drying on the preservation of protein interactions and positions. Cryoelectron microscopy of frozen-hydrated samples offers a means of

Received for publication 24 March 1999 and in final form 10 May 1999.

Address reprint requests to William Lehman, Department of Physiology, Boston University School of Medicine, 80 East Concord Street, Boston, MA 02118. Tel.: 617-638-4397; Fax: 617-638-4273; E-mail: Lehman@med-rana.bu.edu.

C. Xu's current address is Skirball Institute for Biomolecular Medicine, New York University Medical Center, New York, NY 10016.

Abbreviations used: F-actin, filamentous actin; EGTA, ethyleneglycol bis-(β-aminoethylether)-*N,N′*-tetraacetic acid; EM, electron microscopy; SD, standard deviation; S-1, myosin subfragment 1.

0006-3495/99/08/985/08 $2.00

overcoming these concerns because it permits elucidation of structures in a near-native state (with no fixation, staining, or drying). However, 3-D reconstruction of cryo-EM data has not been effective in resolving tropomyosin in all states examined. By using cryo-EM, tropomyosin was resolved in the myosin-induced state (Milligan et al., 1990) and in the Ca^{2+}-state (R. A. Milligan, personal communication), but not in the off-state, raising the objection that tropomyosin may be disordered in the relaxed state and thus might not act as a steric inhibitor. If so, this would imply that the use of the negative staining procedure itself may have artifactually trapped disordered tropomyosin on actin's outer domain in the off-state. We have excluded this possibility in the current study, where we have examined reconstituted thin filaments by cryo-EM and 3-D reconstruction, and have demonstrated that tropomyosin can, in fact, be resolved under relaxing conditions. In addition, we show that tropomyosin strands occupy positions very close to those previously determined by negative staining, hence strongly supporting the steric model of regulation.

MATERIALS AND METHODS

Protein preparation

Bovine cardiac troponin and tropomyosin and rabbit skeletal muscle F-actin were purified as described previously (Tobacman and Adelstein, 1986; Spudich and Watt, 1971). Thin filaments were reconstituted by first combining troponin and tropomyosin and then adding F-actin to the mixture to final concentrations of 7.5, 7.5, and 24 μM, respectively. Reconstitution was carried out in solutions consisting of 100 mM NaCl, 3 mM $MgCl_2$, 0.2 mM EGTA, 1 mM NaN_3, 5 mM PIPES/sodium phosphate buffer (pH 7.1), with or without $CaCl_2$ added to 0.4 mM. Filaments were allowed to incubate at room temperature (~25°C) for 5–10 min before making a 20-fold dilution with additional buffer and then applying the diluted samples to grids for electron microscopy.

Cryoelectron microscopy and helical reconstruction

Freezing was carried out at room temperature in a chamber at 85% relative humidity to minimize changes in salt concentration due to evaporation after blotting. Five μl of filaments was applied to "holey" carbon-coated copper grids that had been glow-discharged in air. After 30 s, grids were blotted from both sides by squeezing between two layers of Whatman #40 filter paper for 1–2 s and then immediately plunged into a 2:1 mixture of liquid ethane and propane cooled by liquid nitrogen. Frozen grid samples were stored in liquid nitrogen until use. A Gatan transfer system and cryoholder (Model 626) were used to transfer grids to a Philips CM120 cryoelectron microscope equipped with a Philips sandwich blade anticontaminator. Images of filaments over holes were recorded at a nominal magnification of 35,000× at 120 kV with a defocus of between 1.6 and 2.0 μm and an electron dose of ~10 e^-/~10e^-/Å^2. Micrographs were digitized with an Eikonix 1412 CCD camera with a pixel size corresponding to 0.71 nm in the micrographs. Filaments were chosen for analysis from areas close to the periphery of holes, where ice was relatively thick and minimal evaporation presumably had occurred during the plunging of grids after blotting. Only filaments with diameters wider than ~15 nm were chosen for analysis because narrower ones frequently do not show tropomyosin in reconstructions (Lehman et al., 1995). Curved filaments were straightened by applying spline-fitting algorithms (Egelman, 1986). Helical reconstruction was carried out by standard methods (DeRosier and Moore, 1970; Amos, 1975; Amos and Klug, 1975; Owen et al., 1996) as described previously (Vibert et al., 1993, 1997). The statistical significance of densities in maps was computed from the standard deviations associated with contributing points using a Student's *t*-test (Milligan and Flicker, 1987; Trachtenberg and DeRosier, 1987). Layer-line data extended to a resolution of 3.5–3.6 nm as estimated by the method of Owen and DeRosier (1993), and no data were collected beyond 2.75 nm. Significant data fell within the first node of the contrast transfer function and no phase or amplitude corrections were applied (Milligan and Flicker, 1987; Milligan et al., 1990). Information on troponin is not acquired by the methods applied (cf. Milligan and Flicker, 1987). Fitting of the atomic structure of F-actin into our maps was carried out (McGough and Way, 1995) as described previously (Lehman et al., 1997). Maps were displayed using the program O (Jones et al., 1991) and a Silicon Graphics INDIGO II imaging system as detailed elsewhere (Vibert et al., 1997). Surface rendering of reconstructions was performed using AVS5 3-D visualization software (Advanced Visual Systems, Inc., Waltham, MA). For the purposes of comparison, electron microscopy and helical reconstruction were performed on filament samples negatively stained with 1% uranyl acetate as previously described (Moody et al., 1990; Vibert et al., 1993, 1997).

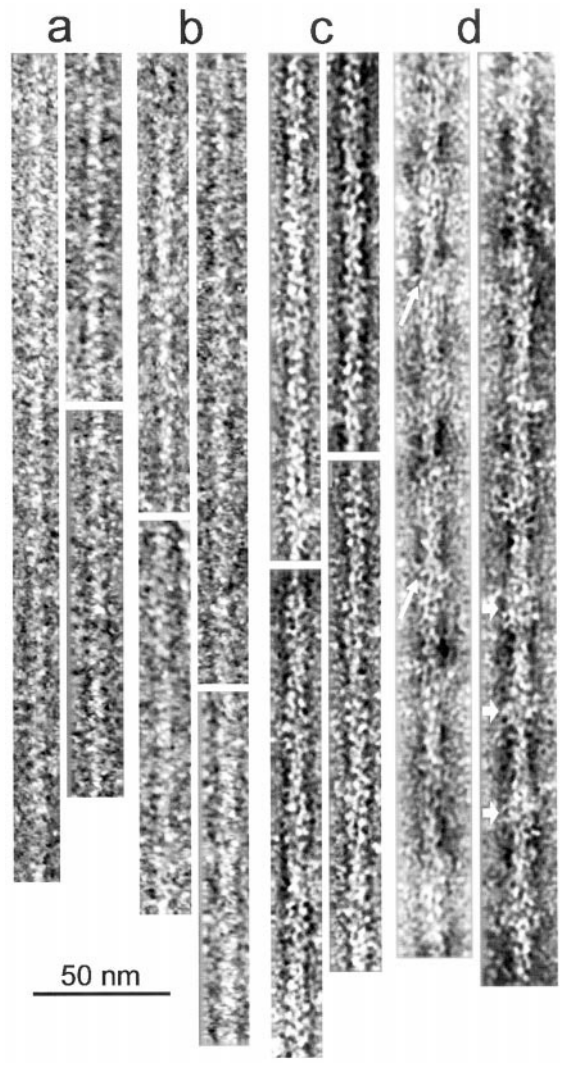

FIGURE 1 Electron micrographs of F-actin and F-actin-troponin-tropomyosin complexes. (*a, b*) Cryopreserved samples; (*c, d*) negatively stained samples; (*a, c*) pure F-actin; (*b, d*) F-actin-troponin-tropomyosin. Note the tropomyosin strands (*narrow arrows*) and troponin bulges (*arrowheads*) in (*d*). Scale bar represents 50 nm.

RESULTS

Inspection of cryoelectron micrographs of reconstituted F-actin-tropomyosin-troponin filaments showed typical double-helical arrays of actin subunits, but no obvious signs of either troponin or tropomyosin, although the filaments were ~10–20% wider in diameter than F-actin controls (Fig. 1, *a* and *b*). Relative to background, unstained frozen-hydrated filaments were inherently low in contrast. This was apparent when they were compared to corresponding negatively stained filaments, which sometimes did display identifiable tropomyosin strands and troponin bulges repeating at 40-nm intervals (Fig. 1, *c* and *d*; cf. Lehman et al., 1994, 1995; Vibert et al., 1997). To detect tropomyosin and determine its position on actin in frozen-hydrated filaments, helical image processing was necessary.

Density maps were calculated from the averaged Fourier transform layer line data (Fig. 2 *b*) obtained from 26 F-actin-tropomyosin-troponin filaments reconstituted and then maintained in EGTA during cryopreservation. The maps revealed actin monomers (Figs. 3 *b* and 4 *a*) whose shape and connectivity were indistinguishable from those in reconstructions of other thin filaments (Milligan et al., 1990; Vibert et al., 1993, 1997; Lehman et al., 1994, 1995). In addition, extra density (tropomyosin) was observed associated with the outer domain of F-actin at an ~3.8 nm radius from the filament center. The extra mass and its location were especially obvious when difference densities computed between maps of F-actin-tropomyosin-troponin and F-actin were superimposed on F-actin reconstructions. These difference densities contoured to the ~2 nm diameter of tropomyosin were significant at confidence levels >99.95% (Fig. 3 *d*). The location of tropomyosin along the length of F-actin filaments is best-visualized in surface views (Fig. 4 *a*) where tropomyosin (*red*) is seen as a continuous strand of density running peripherally along actin filaments (*gold*) associated with subdomain 1 of successive actin monomers and bridging over the shallow aspect of intervening subdomain 2. To define tropomyosin's interactions with thin filaments in more detail, the atomic model of F-actin (Lorenz et al., 1993) was fitted to these reconstructions and substituted for the F-actin densities (Fig. 5). Viewed from the "front" surface of actin (Fig. 5 *a*), tropomyosin (*red wire cage*) can be seen to lie over proposed strong sites of myosin binding (*highlighted in yellow*) and adjacent to but not covering proposed weak sites of myosin binding (*highlighted in white*) (cf. Lehman et al., 1995; Vibert et al., 1997). The point of contact between tropomyosin and the surface of actin in cryo and comparable negatively stained filaments was indistinguishable (Fig. 6 *f*). However, the radial distribution of tropomyosin mass

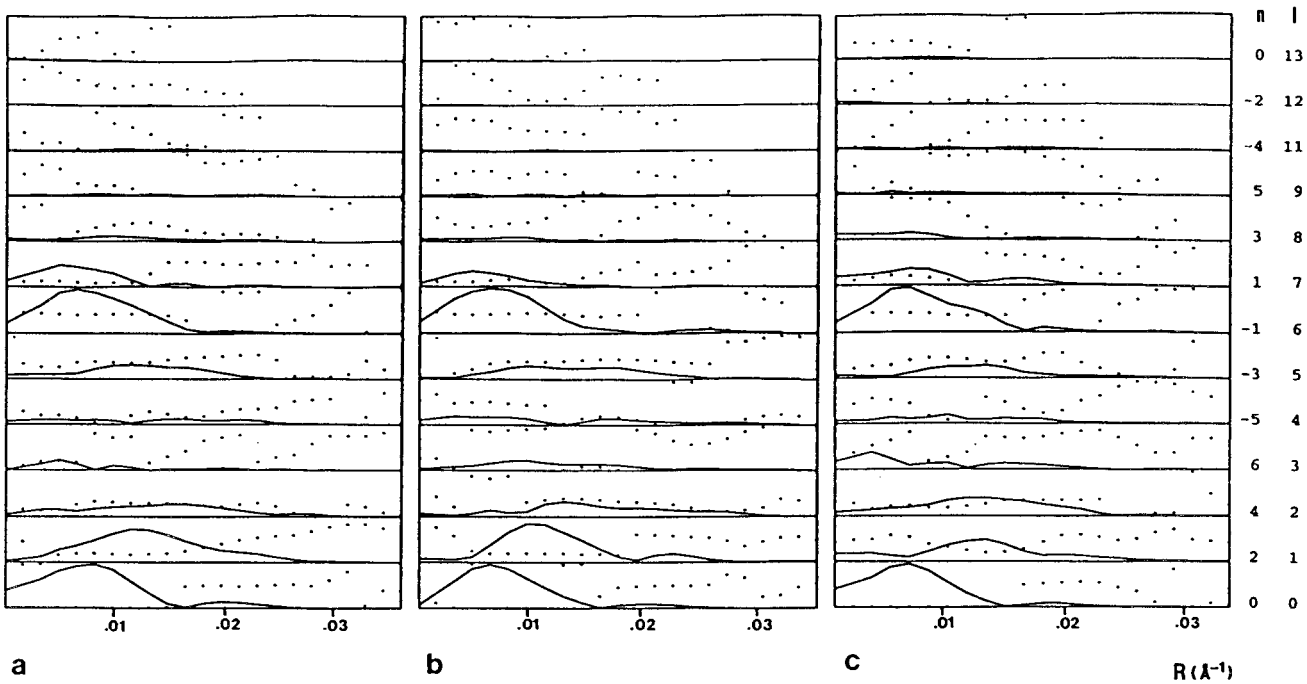

FIGURE 2 Average layer-line data derived from Fourier transforms of cryoimages of (*a*) 20 F-actin filaments; (*b*) 26 F-actin-troponin-tropomyosin filaments maintained in EGTA; (*c*) 15 F-actin-troponin-tropomyosin filaments treated with Ca^{2+}. Amplitudes are represented as continuous lines, and phases (0–360°) as broken lines. Rotational (Bessel) order (*n*) and layer-line numbers (*l*) allowed by the 13/6 actin-helical symmetry imposed on the data are shown; resolution extended to ~3.5 nm in both axial and radial directions. Phase residuals ($\psi \pm$ SD) between individual filament layer-line data sets and the average of the data, a measure of the accuracy of filament alignment, were 53.7 ± 6.4°, 64.1 ± 5.2°, and 59.7 ± 8.1°, respectively; the up-down phase residuals ($\Delta\psi \pm$ SD), a measure of filament polarity, were 18.2 ± 7.3°, 12.2 ± 6.1°, 17.3 ± 9.6°. Note that relative to the first layer line ($l = 1$), the amplitude of peaks along the second layer line ($l = 2$) are greater in the pattern associated with the Ca^{2+}-treated than the EGTA-treated filaments. This presumably reflects a change in the structure's fourfold symmetry, consistent with results of x-ray diffraction on intact muscle (cf. Squire and Morris, 1998).

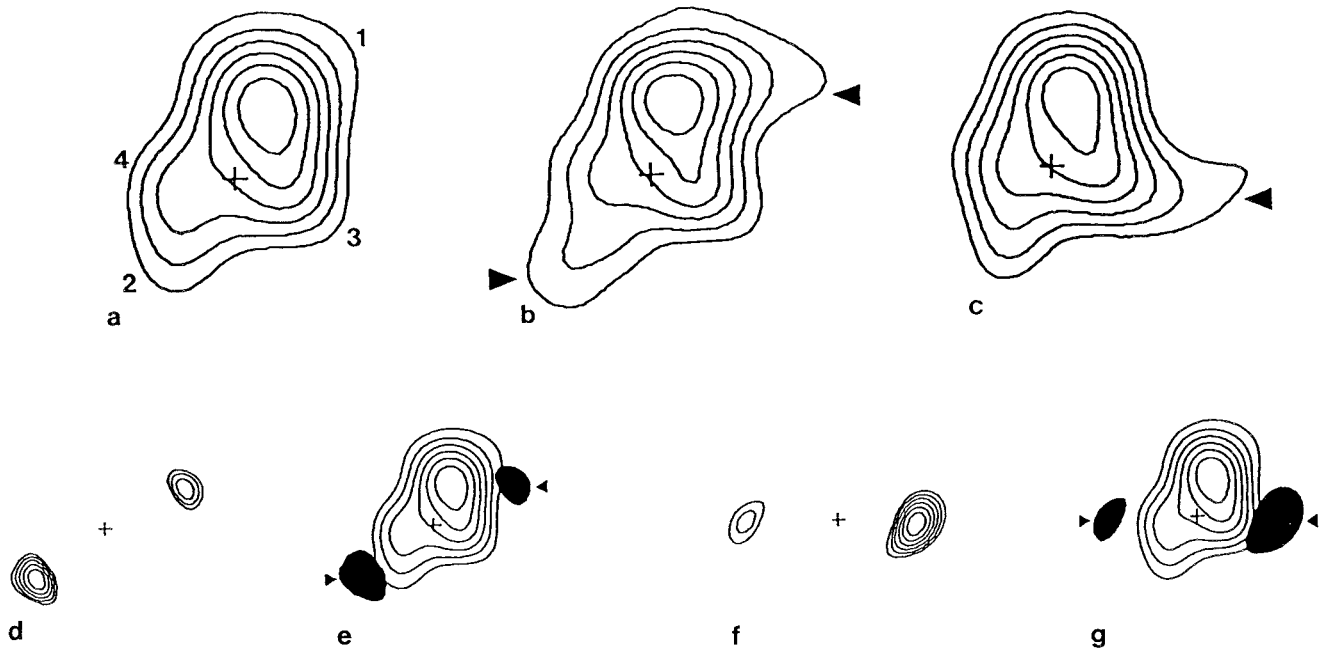

FIGURE 3 (*a–c*) Transverse sections ("*z*-sections") through maps of 3-D reconstructions of cryopreserved thin filaments. Sections shown are at the same relative axial position along respective reconstructions and have the same orientation. Because adjacent actin monomers on either side of the filament axis are staggered, sectioning through the center of actin subdomains 1 and 3 of one actin monomer results in sectioning through subdomains 2 and 4 of the other. (*a*) F-actin, subdomains 1–4 are labeled. (*b*) EGTA-treated F-actin-troponin-tropomyosin; note the extra density (*bold arrows*) associated with actin subdomains 1 and 2, i.e., on the outer domains of the actin monomers. (*c*) Ca^{2+}-treated F-actin-troponin-tropomyosin; note the extra density (*bold arrow*) associated with actin subdomain 3, i.e., on the inner domain of actin (extra density is also present on subdomain 4 of the adjacent monomer but not visible at the contour level chosen for display). (*d–g*) Difference density analysis of reconstructions (note scale is different from *a–c*). (*d, f*) Tropomyosin difference densities derived by subtracting maps of F-actin from those of actin-troponin-tropomyosin filaments; tropomyosin densities from filaments in EGTA (*d*) and Ca^{2+} (*f*) were then superimposed on the map of F-actin (*e*) EGTA; (*g*) Ca^{2+}, where tropomyosin is filled in black. Note that the position of the difference densities has obviously changed from outer to inner domains of F-actin on Ca^{2+}-treatment. The difference densities shown for EGTA- and Ca^{2+}-treated filaments were of high statistical significance (>99.95% and >99.5% confidence levels, respectively). The densities, located 3.8 nm from the central filament axis, accounted for the ~2.0 nm diameter of tropomyosin in each state. Note: in generating thin filament reconstructions, actin was contoured to approximate its known volume, and insignificant low-density information at its edges was omitted. This process can compromise clear delineation of superficially localized actin binding proteins, which also may be of low density (Hanein et al., 1997; Lehman et al., 1997), as tropomyosin was in this case. The procedure of subtracting actin (and its low-density edge information) from thin filament reconstructions allowed low-density tropomyosin information to be isolated, clearly delineating its position.

differed slightly in the two, possibly reflecting differences in resolution or flattening onto the actin backbone that may have happened during drying of negative stain (Fig. 6 *e*). These differences were especially evident when helical projections of reconstructions were compared (Fig. 6, *a–c*). Negatively stained tropomyosin appeared more elongated and narrow in section and at an ~10% smaller (~3.4 nm) radius from the center of the filament (Fig. 6, *d–f*).

To determine whether the Ca^{2+}-induced movement of tropomyosin observed by negative staining (Lehman et al., 1994) also occurs under more native conditions of cryoelectron microscopy, we compared the above reconstructions with ones made from filaments treated with Ca^{2+}. Density maps calculated from averaged layer line data (Fig. 2 *c*) of 15 Ca^{2+}-treated filaments revealed actin monomer shape and connectivity very similar to those seen in EGTA-treated filaments (Fig. 3 *c*). However, these maps showed additional tropomyosin density at an ~3.8 nm radius now on the inner domain of actin, which again became even more obvious after difference density analysis (Figs. 3, *f* and *g,* and 6 *g*) and surface rendition (Fig. 4 *b*). Here tropomyosin was associated with subdomain 3 of successive actin monomers bridging over intervening subdomains 4 (Figs. 3, *c* and *g,* and 4 *b*). Fitting to the molecular model of F-actin showed that tropomyosin was displaced from most of the strong myosin binding sites. Its outer edge was located adjacent to the subdomain 1/3 junction, near or over only one set of strong myosin binding residues at positions 332–334 in the actin sequence (Fig. 5 *b*; cf. Lehman et al., 1994; Vibert et al., 1997) where the tip of myosin is found once bound to actin (Rayment et al., 1993b; Vibert et al., 1997). The point of contact between tropomyosin and the surface of actin in cryopreserved and in negatively stained filaments that had been treated with Ca^{2+} was indistinguishable (Fig. 6 *g*).

DISCUSSION

By using cryoelectron microscopy and image analysis of unstained frozen-hydrated filaments, we have for the first

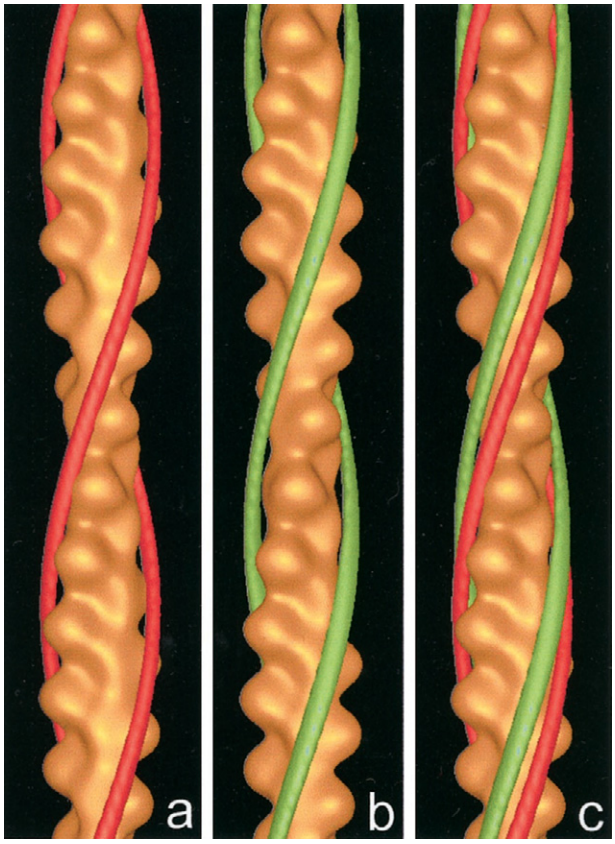

FIGURE 4 Surface views of reconstructions of thin filaments showing the positions of tropomyosin strands superimposed on actin in (*a*) EGTA and (*b*) Ca^{2+}. In (*c*) tropomyosin strands associated with both EGTA and Ca^{2+} positions are superimposed on actin for comparison. Reconstructions show characteristic bilobed actin (*gold*) and continuous tropomyosin strands. In EGTA, tropomyosin (*red*) occupies a position on the inner edge of the outer domain of actin, whereas in Ca^{2+}, tropomyosin (*green*) lies along the outer edge of the inner domain. Surface rendering was carried out by superimposing tropomyosin strand densities obtained by difference analysis on the maps of pure F-actin.

time resolved tropomyosin density in reconstructions of thin filaments under near-native relaxing conditions. We also demonstrated that tropomyosin moves to a new position under high Ca^{2+}-activating conditions; R. A. Milligan (personal communication) also finds a similar high-Ca^{2+} position. Our data show that tropomyosin is discretely localized, in both high and low Ca^{2+} conditions, in the positions previously suggested by negative staining (Lehman et al., 1994, 1995; Vibert et al., 1997), providing further support for the steric model of muscle regulation. Our reconstructions argue against the notion that negative stain traps tropomyosin artifactually in one or another position or that tropomyosin in relaxed filaments is disordered. If tropomyosin were dynamically disordered between closely located on- and off-states, its density in reconstructions would be diffuse and not discretely localized, contrary to observation; were the disorder over considerably larger distances, tropomyosin density would tend to disappear. Although tropomyosin appears to occupy a preferred position in a given state, the possibility of a dynamic equilibrium between states (cf. Phillips et al., 1986) with one such state dominating *on average* cannot be easily addressed by the methods used.

Fitting our cryoreconstructions to the atomic model of F-actin substantiates results previously obtained on negatively stained samples. In the off-state, tropomyosin is located over amino acid residues thought to participate in strong myosin binding required for cross-bridge cycling (cf. Rayment et al., 1993b). Sterically blocking access of myosin heads to these sites would necessarily inhibit muscle activity by interfering with the transition myosin undergoes from weak to strong binding on actin.

We attribute our ability to resolve tropomyosin in the off-state to the conditions we used to prepare our samples for electron microscopy, and not to anything unique about our image processing procedures, which were routine. For reasons that are not well-understood, binding interactions of proteins are weakened during cryopreservation (Rost et al., 1998). This problem is exacerbated in our studies, where end-to-end bonded tropomyosin strands interacting electrostatically with actin (Lorenz et al., 1995) may dissociate cooperatively at the low protein concentrations used for electron microscopy. We attempted to maximize tropomyosin binding to thin filaments by using ionic conditions that optimized tropomyosin-actin binding, namely 100 mM NaCl and 3 mM $MgCl_2$ (Eaton et al., 1975). We also attempted to ensure troponin-tropomyosin saturation and to diminish dissociation from F-actin by maintaining a twofold molar excess of troponin-tropomyosin over that bound stoichiometrically by F-actin. Higher amounts than this were avoided, as they sometimes led to additional densities being observed on the extreme periphery of actin near its N-terminus, possibly due to extrastoichiometric binding of troponin (cf. Levine et al., 1988). Our previous observations of tropomyosin in on and off positions were by negative staining of *native* thin filaments (Lehman et al., 1994, 1995; Vibert et al., 1997). Our observations of tropomyosin in distinct positions here, using negative staining and cryo-EM of *reconstituted* filaments, show that native filaments are not required for visualization of tropomyosin. In fact, respective tropomyosin positions in reconstituted bovine cardiac muscle filaments are indistinguishable from those also found for native filaments from *Limulus* telson muscle (Lehman et al., 1994; Vibert et al., 1997) and frog skeletal and cardiac muscle (Lehman et al., 1995; Vibert et al., 1997).

The agreement between the thin filament reconstructions obtained from both cryo-EM and negative staining data lends validity to the use of both methods. The two techniques each have advantages and disadvantages, and in studies such as ours provide complementary information. Cryo-EM is powerful because it permits preservation of proteins in as close to their native configuration as is currently possible. However, the inherent low contrast of cryo-EM makes image analysis difficult, particularly for flexible structures such as undecorated (S-1-free) thin fila-

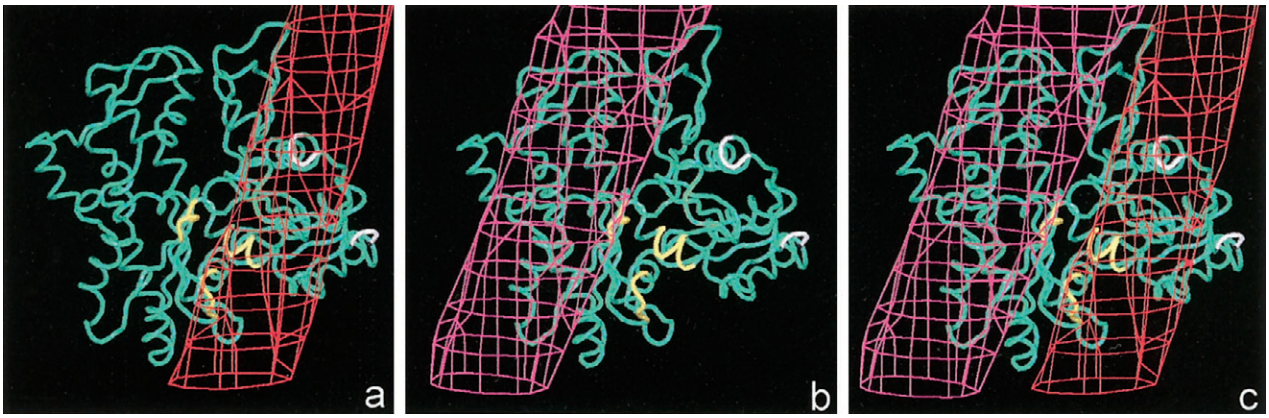

FIGURE 5 Location of tropomyosin densities on the atomic structure of F-actin. Here the atomic model of F-actin (Lorenz et al., 1993) was fitted to our EM reconstructions and the respective positions of tropomyosin determined. A single actin monomer from the atomic model was substituted for actin in our EM maps and only tropomyosin difference densities displayed. The atomic model of F-actin is depicted as a green α-carbon chain with clusters of amino acids thought to be involved in strong myosin binding (representing residues 144–148, 332–334, 340–346; Rayment et al., 1993b) highlighted in yellow and those in weak myosin binding (representing residues 1–4 and 92–95; Miller et al., 1995) highlighted in white. Were actin decorated with myosin in rigor, myosin heads would approach actin from the lower right corner of the figures (Milligan et al., 1990; Rayment et al., 1993b; Vibert et al., 1997). (*a*) Filaments treated with EGTA; tropomyosin (*red wire cage*) lies over several strong myosin binding sites, presumably blocking access of myosin heads. However, N-terminal amino acids (*highlighted in white on subdomain 1*) and residues 92–95 (*highlighted in white on subdomain 2*) involved in weak prepower stroke myosin contacts (Miller et al., 1995) remain exposed. Accessibility of the latter sites is particularly manifest in transverse view (data not shown). (*b*) Filaments treated with Ca^{2+}; tropomyosin (*pink wire cage*) has moved onto the inner domain of actin and most of the myosin binding interface is exposed. However, the outer edge of tropomyosin remains positioned near or over residues 332–334 (amino acid cluster highlighted in yellow in the center of *b* at the junction of subdomains 1 and 3). Other studies (Vibert et al., 1997) have shown that strong myosin binding causes a further displacement of tropomyosin from this Ca^{2+}-induced location. In (*c*) tropomyosin positions associated with both EGTA and Ca^{2+} positions are shown for comparison.

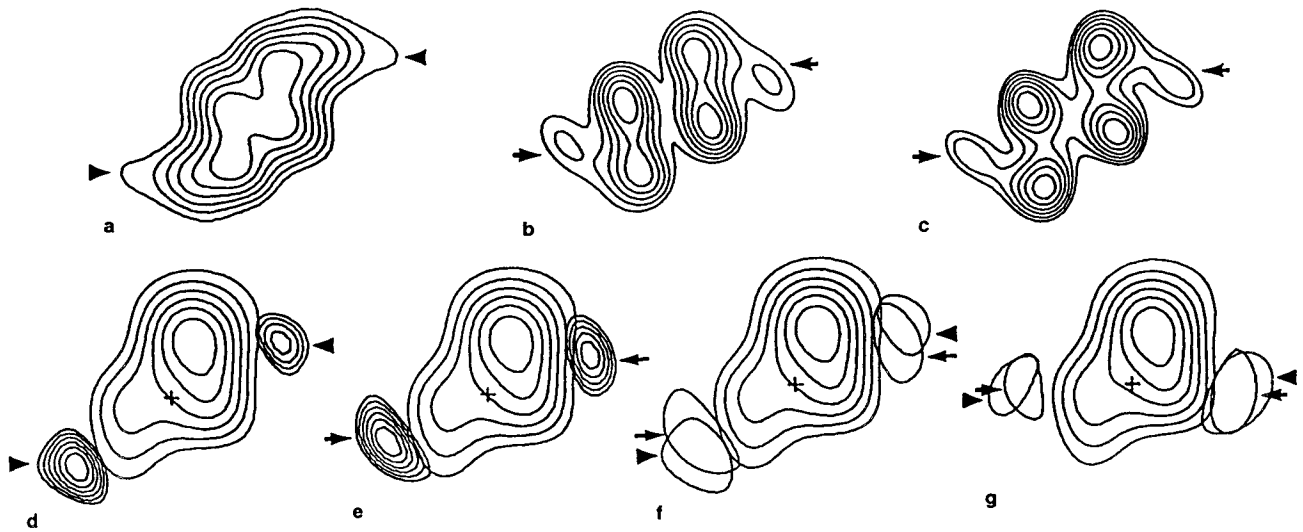

FIGURE 6 Location of tropomyosin-actin contacts by cryo-EM and negative staining. (*a–c*) Helical projections of reconstructions formed by projecting component densities down the long-pitch actin helices (i.e., along the $n = 2$ helical tracks) onto a plane perpendicular to the filament axis. Such projected images suggest differences between tropomyosin orientation in cryopreserved and negatively stained samples. (*a*) Cryoreconstruction of reconstituted thin filaments in EGTA. (*b, c*) Reconstructions of negatively stained filaments; (*b*) reconstituted thin filaments; (*c*) isolated "native" (frog) thin filaments (Lehman et al., 1995) in EGTA. Note that the tropomyosin densities (*arrows*) associated with the negative stained filaments are more elongated than those of frozen-hydrated filaments (*arrowheads*). To investigate the possibility that the two methods might produce different actin-tropomyosin contact sites, difference density analysis was carried out as above where tropomyosin densities from reconstructions of negatively stained and cryopreserved filaments treated with EGTA were aligned to and superimposed on the reconstruction of frozen-hydrated F-actin for comparison (*d–f*; cf. Fig. 3 *e*). The distinctions noted above again are evident; stained tropomyosin is narrower and more asymmetric, but appears to contact actin at virtually the same site as frozen-hydrated tropomyosin. Tropomyosin from (*d*) cryo-EM; (*e*) negative staining; (*f*) tropomyosin from both sources superimposed on actin for comparison (tropomyosin marked as above); in (*f*) only the outermost contour of the respective tropomyosin densities is displayed to help in distinguishing relative shapes. The same analysis was carried out for reconstituted filaments treated with Ca^{2+}. In (*g*) tropomyosin difference densities derived from negatively stained and cryopreserved filaments were aligned and then both superimposed on the reconstruction of frozen-hydrated F-actin for comparison, as in (*f*). Tropomyosin from cryo-EM (*arrowheads*) and from negatively staining (*arrows*) again contact actin at the same site, now on the inner domain of actin. Negatively stained tropomyosin appears to be slightly closer to actin than cryotropomyosin, but the difference is small.

ments. The low signal-to-noise ratio increases the chance of making small errors during data processing (e.g., in filament straightening and precise boxing) and this, compounded with the relatively large defocus used in recording cryoimages, can ultimately limit the resolution obtained for reconstructions of such filaments (cf. Orlova and Egelman, 1995). Negative staining of filaments has also proved to be a powerful tool and allows more straightforward analysis of filament structure. On extremely ordered structures, it can give relatively high-resolution reconstructions. Staining of the F-actin-scruin complex, for example, yielded reconstructions with 1.3-nm resolution (Owen and DeRosier, 1993). The method has also been invaluable in revealing subtle variation in F-actin subdomain conformation (Egelman and Orlova, 1995) and in defining the transition between Ca^{2+}- and myosin-induced thin filament states (Vibert et al., 1997). The similarity we have observed between thin filament reconstructions obtained from cryo-EM and negative stain data lends strong credibility to the use of the relatively simpler negative staining approach for studies of thin filament ultrastructure. Our work also shows that, despite difficulties encountered when using cryo-EM, changes in thin filament ultrastructure can be determined under near-native solution conditions.

The authors thank Peter Vibert for teaching us how to prepare frozen-hydrated samples, for critically reading the manuscript, and for his encouragement. We are grateful to C. A. Landis and C. Butters for production of proteins and N. Gherbesi for photographic help.

This work was funded by National Institutes of Health Research Grants HL36153 (to W.L.), AR34711 (to R.C.), and HL38834 (to L.T.), and National Institutes of Health Shared Instrumentation Grant RR08426 (to R.C.) supporting electron microscope facilities.

REFERENCES

AL-Khayat, H. A., N. Yagi, and J. M. Squire. 1995. Structural changes in actin-tropomyosin during muscle regulation: computer modeling of low-angle x-ray diffraction data. *J. Mol. Biol.* 252:611–632.

Amos, L. A. 1975. Combination of data from helical particles: correlation and selection. *J. Mol. Biol.* 99:65–73.

Amos, L. A., and A. Klug. 1975. Three-dimensional image reconstruction of the contractile tail of T4 bacteriophage. *J. Mol. Biol.* 99:51–73.

Bremel, R. D., J. M. Murray, and A. Weber. 1972. Cooperative behavior in actin. *Cold Spring Harbor Symp. Quant. Biol.* 37:267–275.

DeRosier, D. J., and P. B. Moore. 1970. Reconstruction of three-dimensional images from electron micrographs of structures with helical symmetry. *J. Mol. Biol.* 52:355–369.

Eaton, B. L., D. R. Kominz, R. Tsukui, and E. Eisenberg. 1975. Correlation between the inhibition of the acto-heavy meromyosin ATPase and the binding of tropomyosin to F-actin: effects of Mg^{2+}, KCl, troponin-I, and troponin-C. *Biochemistry*. 14:2718–2724.

Egelman, E. H. 1986. An algorithm for straightening images of curved filamentous structures. *Ultramicroscopy*. 19:367–374.

Egelman, E. H., and A. Orlova. 1995. Allostery, cooperativity, and different structural states of F-actin. *J. Struct. Biol.* 115:159–162.

Hanein, D., P. Matsudaira, and D. J. DeRosier. 1997. Evidence for a conformational change in actin induced by fimbrin (N375) binding. *J. Cell Biol.* 139:387–396.

Haselgrove, J. C. 1972. X-ray evidence for a conformational change in actin-containing filaments of vertebrate striated muscle. *Cold Spring Harbor Symp. Quant. Biol.* 37:341–352.

Holmes, K. C. 1995. The actomyosin interaction and its control by tropomyosin. *Biophys. J.* 68(Suppl.):2–7.

Holmes, K. C. 1997. The swinging lever-arm hypothesis of muscle contraction. *Curr. Biol.* 7:R112–R118.

Holmes, K. C., and W. Kabsch. 1991. Muscle proteins: actin. *Curr. Opin. Struct. Biol.* 1:270–280.

Huxley, H. E. 1972. Structural changes in actin- and myosin-containing filaments during contraction. *Cold Spring Harbor Symp. Quant. Biol.* 37:361–376.

Jones, T. A., J. Y. Zou, S. W. Cowan, and M. Kjeldgaard. 1991. Improved methods for the building of protein models in electron density maps and the location of errors in these models. *Acta Crystallogr., Sect. A.* 47: 110–119.

Kress, M., H. E. Huxley, A. R. Faruqi, and J. Hendrix. 1986. Structural changes during activation of frog muscle studied by time-resolved x-ray diffraction. *J. Mol. Biol.* 188:325–342.

Landis, C. A., A. Bobkova, E. Homsher, and L. Tobacman. 1997. The active state of the thin filament is destabilized by an internal deletion in tropomyosin. *J. Biol. Chem.* 272:14051–14056.

Lehman, W., R. Craig, and P. Vibert. 1994. Ca^{2+}-induced tropomyosin movement in *Limulus* thin filaments revealed by three dimensional reconstruction. *Nature*. 368:65–67.

Lehman, W., P. Vibert, and R. Craig. 1997. Visualization of caldesmon on smooth muscle thin filaments. *J. Mol. Biol.* 274:310–317.

Lehman, W., P. Vibert, P. Uman, and R. Craig. 1995. Steric-blocking by tropomyosin visualized in relaxed vertebrate muscle thin filaments. *J. Mol. Biol.* 251:191–196.

Lehrer, S. S. 1994. The regulatory switch of the muscle thin filament: Ca^{2+} or myosin heads? *J. Muscle Res. Cell Motil.* 15:232–236.

Lehrer, S. S., and M. A. Geeves. 1998. The muscle thin filament as a classical cooperative/allosteric regulatory system. *J. Mol. Biol.* 277: 1081–1089.

Lehrer, S. S., and E. P. Morris. 1982. Dual effects of tropomyosin and troponin-tropomyosin on subfragment 1 ATPase. *J. Biol. Chem.* 257: 8073–8080.

Levine, B. A., A. J. Moir, and S. V. Perry. 1988. The interaction of troponin-I with the N-terminal region of actin. *Eur. J. Biochem.* 172: 389–397.

Lorenz, M., K. J. V. Poole, D. Popp, G. Rosenbaum, and K. C. Holmes. 1995. An atomic model of the unregulated thin filament obtained by x-ray fiber diffraction on oriented actin-tropomyosin gels. *J. Mol. Biol.* 246:108–119.

Lorenz, M., D. Popp, and K. C. Holmes. 1993. Refinement of the F-actin model against x-ray fiber diffraction data by use of a directed mutation algorithm. *J. Mol. Biol.* 234:826–836.

McGough, A., and M. Way. 1995. Molecular model of an actin filament capped by a severing protein. *J. Struct. Biol.* 115:144–150.

McKillop, D. F. A., and M. A. Geeves. 1993. Regulation of the interaction between actin and myosin subfragment-1. Evidence for three states of the thin filament. *Biophys. J.* 65:693–701.

Miller, C. J., P. Cheung, P. White, and E. Reisler. 1995. Actin's view of the actomyosin interface. *Biophys. J.* 68(Suppl):50–56.

Milligan, R. A., and P. F. Flicker. 1987. Structural relationships of actin, myosin, and tropomyosin revealed by cryo-electron microscopy. *J. Cell Biol.* 105:29–39.

Milligan, R. A., M. Whittaker, and D. Safer. 1990. Molecular structure of F-actin and the location of surface binding sites. *Nature*. 348:217–221.

Moody, C., W. Lehman, and R. Craig. 1990. Caldesmon and the structure of vertebrate smooth muscle thin filaments: electron microscopy of isolated thin filaments. *J. Muscle Res. Cell Motil.* 11:176–185.

Orlova, A., and E. H. Egelman. 1995. Structural dynamics of F-actin. I. Changes in the C terminus. *J. Mol. Biol.* 245:582–597.

Owen, C., and D. J. DeRosier. 1993. A 13-Å map of the actin-scruin filament from the *Limulus* acrosomal process. *J. Cell Biol.* 123:337–344.

Owen, C., D. G. Morgan, and D. J. DeRosier. 1996. Image analysis of helical objects: the Brandeis helical package. *J. Struct. Biol.* 116: 167–175.

Parry, D. A. D., and J. M. Squire. 1973. Structural role of tropomyosin in muscle regulation: analysis of the x-ray patterns from relaxed and contracting muscles. *J. Mol. Biol.* 75:33–55.

Phillips, G. N., Jr., J. P. Fillers, and C. Cohen. 1986. Tropomyosin crystal structure and muscle regulation. *J. Mol. Biol.* 192:111–131.

Poole, K. J. V., G. Evans, G. Rosenbaum, M. Lorenz, and K. C. Holmes. 1995. The effect of crossbridges on the calcium sensitivity of the structural change of the regulated thin filament. *Biophys. J.* 68:365*a*. (Abstr.).

Rayment, I., H. M. Holden, M. Whittaker, C. B. Yohn, M. Lorenz, K. C. Holmes, and R. A. Milligan. 1993b. Structure of the actin-myosin complex and its implications for muscle contraction. *Science*. 261: 58–65.

Rayment, I., W. R. Rypniewski, K. Schmidt-Bäse, R. Smith, D. R. Tomchick, M. M. Benning, D. A Winkelmann, G. Wesenberg, and H. M. Holden. 1993a. Three-dimensional structure of myosin subfragment-1: a molecular motor. *Science*. 261:50–58.

Rost, L. E., D. Hanein, and D. J. DeRosier. 1998. Reconstruction of symmetry deviations: a procedure to analyze partially decorated F-actin and other incomplete structures. *Ultramicroscopy*. 72:187–197.

Spudich, J. A., and S. Watt. 1971. The regulation of rabbit skeletal muscle contraction. I. Biochemical studies of the interaction of the tropomyosin-troponin complex with actin and the proteolytic fragments of myosin. *J. Biol. Chem.* 242:4866–4871.

Squire, J. M., and E. P. Morris. 1998. A new look at thin filament regulation in vertebrate skeletal muscle. *FASEB J.* 12:761–771.

Tobacman, L. S., and R. S. Adelstein. 1986. Mechanism of regulation of cardiac actin-myosin subfragment-1 by troponin-tropomyosin. *Biochemistry*. 25:798–802.

Trachtenberg, S., and D. J. DeRosier. 1987. Three-dimensional structure of frozen hydrated flagellar filament of *Salmonella typhimurium. J. Mol. Biol.* 195:581–601.

Vibert, P., R. Craig, and W. Lehman. 1993. Three-dimensional reconstruction of caldesmon-containing smooth muscle thin filaments. *J. Cell Biol.* 123:313–321.

Vibert, P., R. Craig, and W. Lehman. 1997. Steric-model for activation of muscle thin filaments. *J. Mol. Biol.* 266:8–14.